Lab on a Chip

Accepted Manuscript

This is an *Accepted Manuscript*, which has been through the RSC Publishing peer review process and has been accepted for publication.

Accepted Manuscripts are published online shortly after acceptance, which is prior to technical editing, formatting and proof reading. This free service from RSC Publishing allows authors to make their results available to the community, in citable form, before publication of the edited article. This *Accepted Manuscript* will be replaced by the edited and formatted *Advance Article* as soon as this is available.

To cite this manuscript please use its permanent Digital Object Identifier (DOI®), which is identical for all formats of publication.

More information about *Accepted Manuscripts* can be found in the **Information for Authors**.

Please note that technical editing may introduce minor changes to the text and/or graphics contained in the manuscript submitted by the author(s) which may alter content, and that the standard **Terms & Conditions** and the **ethical guidelines** that apply to the journal are still applicable. In no event shall the RSC be held responsible for any errors or omissions in these *Accepted Manuscript* manuscripts or any consequences arising from the use of any information contained in them.

RSC Publishing

www.rsc.org/loc
Registered Charity Number 207890

Single-molecule mobility in confined and crowded femtolitre chambers

Jason D. Fowlkes and C. Patrick Collier

Graphical abstract:

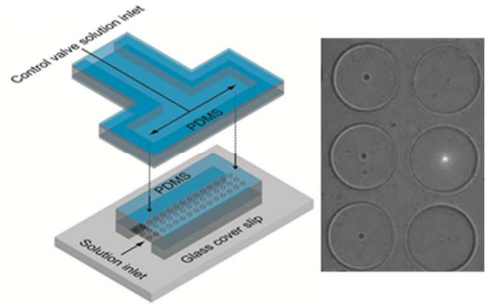

The effects of increased crowding and confinement on the mobility of individual fluorescent molecules were studied using Fluorescence Correlation Spectroscopy and a microfluidic device with sealable femtolitre-volume chambers, and compared to three dimensional Monte Carlo simulations.

Cite this: DOI: 10.1039/c0xx00000x

www.rsc.org/xxxxxx

ARTICLE TYPE

Single-molecule mobility in confined and crowded femtolitre chambers

Jason D. Fowlkes[a] and C. Patrick Collier*[a]

Received (in XXX, XXX) Xth XXXXXXXXX 20XX, Accepted Xth XXXXXXXXX 20XX
DOI: 10.1039/b000000x

The effects of increased crowding and confinement on the mobility of individual fluorescent molecules were studied using Fluorescence Correlation Spectroscopy (FCS) in a microfluidic device with sealable femtoliter-volume chambers, and compared to three dimensional stochastic Monte Carlo simulations. When crowding and the degree of confinement were increased simultaneously, extended correlation times of fluorescent intensity fluctuations were observed with FCS compared to varying either crowding or confinement alone. Both experimental data and simulation suggest these extended correlation times were due to increased fluorophore adsorption-desorption events at the chamber lid in the presence of crowders. The data in increasingly confined and crowded chambers described here captures some of the salient features of crowding in cell-like environments.

Introduction

Fluorescence Correlation Spectroscopy (FCS) is a powerful technique for quantifying low concentrations of fluorescent molecules, down to single-molecule limits, and for measuring dynamical properties such as diffusivity.[1-12] Most systems of biological interest are strongly confined and/or crowded, which presents problems for applying standard FCS models appropriate for open detection volumes where boundary effects can be neglected. When FCS experiments are performed in confining volumes approaching that of the probe volume, deviations from the standard model can result due to molecular interactions with walls or interfaces.[13-15]

A number of studies have been published on FCS in confining structures, such as microchannels[16-19] and nanochannels,[20-24] as well as crowded environments such as gels, glasses, lipid membranes and other cellular structures.[25-30] In general, experimental studies on synthetic systems have featured environments confined in one or two dimensions, but not totally closed. Even for the smallest nanochannels, there is still one axial dimension where steady-state free diffusion can take place. Studies on FCS in increasingly crowded environments have also been presented,[21] although, to our knowledge, there has not been to date a systematic FCS study of the combined effects of crowding and confinement, particularly for completely closed systems.

Here, a microfluidic device is described that features arrays of sealable femtoliter-volume chambers ranging in size from 10 to 2 μm that can trap molecules on demand within one second by hydraulically actuating a control valve.[31] Three-dimensional stochastic Monte Carlo simulations were developed to interpret the FCS data. Once sealed, molecules cannot escape the chambers, which results in different behaviour measured with FCS from that seen in micro or nanochannels where freely diffusing molecules can exit or enter the probe volume under steady-state conditions.

By simultaneously increasing the degree of confinement in chambers with increased weight percent of Ficoll-70 crowding agent, extended correlation times of fluorescent fluctuations were observed with FCS compared to varying crowding or confinement alone. Both data and simulation suggest that these extended correlation times result from increased adsorption-desorption events at the chamber lid that occurred due to increases in local, effective concentrations of fluorophores in the presence of crowders. These results are reminiscent to how crowding in cells drives biopolymer assembly via excluded volume effects.[32,33]

Experimental Methods

Microfluidic devices were fabricated in poly-(dimethylsiloxane) (PDMS) using multilayer soft-lithographic techniques. Figure 1 is a schematic of the microfluidic device. Photolithography with diluted SU-8 2015 photoresist (2:1 ratio in SU-8 thinner, Microchem Corp.) was used to fabricate masters on silicon. Arrays of chambers within 160 μm wide microchannels in PDMS were replicated from the masters by micromolding. The chambers were structurally defined by 10 μm wide walls, with inner diameters ranging from 10 μm to 2 μm. A layer of SU-8 was patterned first for the channel, followed by a second layer for the chambers according to the manufacturer's specifications. The height of the SU-8 features on the master used to define the channels was about 8 μm, while that of the microcavities was 5 μm, as measured by a Dektak profilometer.

Control valves in a second PDMS layer were fabricated by micromolding PDMS replicas on silicon masters with 18 μm high features defined in SU-8 2015. Both the control and chamber/channel masters were silanized with trimethylchlorosilane vapor (Aldrich) for 60 minutes in order to facilitate release of the PDMS from the mold after curing.

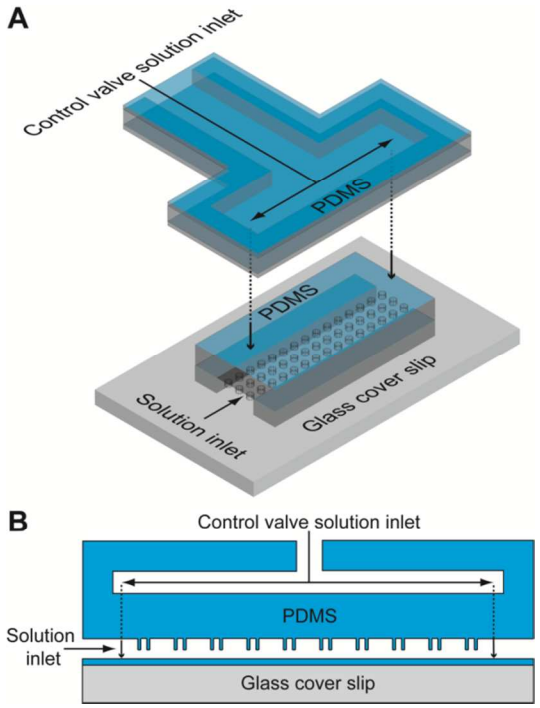

Fig. 1 Schematic of microfluidic device with femtoliter-volume chambers, hydraulically actuated with a control valve in a second PDMS layer.

For the chamber/channel membrane Sylgard 184 PDMS (Dow Corning) with a 20:1 mass ratio of base to curing agent was thoroughly mixed, degassed, and spin-coated onto the mold at 1000 rpm, followed by a partial cure for 5 minutes in an oven at 80° C. For the control valve replica, PDMS with a 5:1 mass ratio of base to curing agent was mixed, degassed, poured onto its mold, degassed again, and partially cured for 15 minutes at 80° C. Holes for the inlets to the control valves were punched with a 0.75 mm hole-puncher (Harris Uni-Core, Ted Pella, Inc.) and then the control valve replica was aligned and bonded to the chamber/channel membrane by additional curing at 80° C for two hours to form a monolithic slab of PDMS. After curing, the combined chamber/channel membrane and control valve replica was peeled off the chamber/channel mold and holes were punched for inlets and outlets to the channels. The combined replica was then bonded to a #1 glass coverslip (Gold Seal, Ted Pella Inc.) that had a 10 μm-thick layer of PDMS spin-coated onto it (10:1 mass ratio of base to curing agent, 6000 rpm) followed by curing for 30 minutes at 120° C. Bonding between the PDMS replica and the PDMS-coated glass coverslip was activated by plasma treatment of both bonding surfaces in an inductively-coupled plasma cleaner at 10.5 W for 20 seconds (Harrick), followed by curing for at least two hours at 80° C.

Alexafluor 555 (AF555) was purchased from Molecular Probes, and Ficoll-70, glucose oxidase, catalase, glucose, β-mercaptoethanol (BME) and phosphate buffered saline (PBS, pH 7.4) were obtained from Sigma Aldrich. Samples were prepared by mixing 10 μL aliquots from a 50 nM stock solution of AF555 with the components of a photobleaching-limiting cocktail,[34] which included 200 μL glucose oxidase (250 nM), 150 μL catalase (64 nM), 200 μL glucose and 100 μL BME, diluted to 10 mL with increasing amounts of Ficoll-70 stock solution (36 wt. percent in PBS) to give a series of solutions containing ~50 pM AF555 and including 0, 5, 10, 20 or 30 wt. percent crowding agent. Each sample was run in a different device to prevent cross contamination between samples.

4 mL glass vials with PTFE/silicone septum lids (C4015-17W, National Scientific) were used as sample reservoirs, and were connected to high precision closed-loop voltage-pressure transducers (Marsh Bellofram) by 24 gauge PTFE tubing (Component Supply Co.). The reservoirs were connected to the inlets of the PDMS device by 23 gauge blunt tip needles. Male-to-male luer lock adapters (Qosina) holding two 23 gauge needles, one penetrating the septum of the vial cap, and the other connecting to the 24 gauge PTFE tubing, were used for access into and out of the sample vials. The pressure regulators were controlled by a custom Matlab script (Mathworks) through an analog output board (16 bit resolution, 0-10 V range, USB3103, Measurement Computing), and were calibrated using a Dwyer Series 475 Mark III digital manometer. After introducing the sample solution into the channel by pressurizing the sample reservoir, the flow was stopped for FCS measurements. The control valve was filled with the same PBS buffer solution used to make the samples, in order to prevent evaporation from the chambers. It was actuated (at 34.5 kPa with N_2 gas pressurizing the PBS reservoir) to deflect the membrane containing the chamber array downward within one second, trapping solution in the cavities as they formed a tight seal on the glass coverslip. The sealing of the chambers was tested by trapping and photobleaching rhodamine dye. No recovery of fluorescence was observed after 10 minutes. When the pressure on the control valve was released, the membrane returned to its initial position and the cavities separated from the glass coverslip, releasing the trapped solution.

Bright field and fluorescent images were acquired with an inverted epifluorescent microscope (Eclipse TE 300, Nikon Instruments), using a 100x oil-immersion objective (N.A. 1.4) and a CCD camera (CoolSNAP-HQ, Roper Scientific) controlled with Metamorph software (Universal Imaging Corp.). Images were analysed with ImageJ software (National Institutes of Health). For FCS, a diode-pumped, solid-state laser operating at 532 nm (LLS-0532-CF, Laserglow Technologies) was spatially filtered to give a Gaussian profile, expanded and collimated (Thor Labs) before being directed onto the back aperture of the 100x objective. Neutral density filters (ND2 and ND3) were used to limit the laser fluence at the focal plane in order to reduce photobleaching. With the ND3 filter the laser power just before the 100x objective was measured at 85 μW. A custom filter set specifically designed for single-molecule detection with 532 nm laser excitation was used (ZET 532/10x excitation, ZT 532rdc dichroic, ET 595/50m emission) (Chroma Technology Corp.). The optical probe volume of the focused laser was calibrated using the known diffusion coefficient of rhodamine 110 (4.3×10^{-6} cm^2/s)[35] to give half-axes of $r_0 = 300$ nm and $z_0 = 1$ μm for the three-dimensional Gaussian intensity profile. Fluorescence bursts from individual dye molecules passing through the optical probe volume were detected with a photon counting module (Perkin-Elmer SPCM-AQR-14). A 50 μm pinhole was placed at the conjugate focal plane before the photon counting module to reduce background fluorescence. Output from the photon

counting module was sent in parallel to a multichannel scaler (MCS-pci, Ortek) for characterizing real-time fluorescence bursts, and to a dual-channel correlator card (Flex5000, Correlator.com) for generating autocorrelation functions (ACF). Using the CCD camera, the laser spot was carefully positioned in the centre of each chamber away from the sidewalls, although the position of the laser spot relative to the lid of the chamber when hydraulically sealed could not be determined.

Simulation Methods

A particle tracking algorithm was used to simulate the random, Brownian motion of the diffusing fluorescent molecules in a virtual cylindrical chamber. The methodology used here is similar to that reported in Ref. [36]. A fictitious laser beam was focused within the simulation domain to excite solute fluorescence and FCS curves were derived from integrated intensity acquisitions taken at Δt_{acq}=204.5ns. Fluorescence correlation curves were derived from a vector of integrated intensity bins according to

$$\boldsymbol{G(\nu)} = \frac{\mathbf{1}}{\boldsymbol{N-\nu}} \sum_{\boldsymbol{i=1}}^{\boldsymbol{N-\nu}} \frac{(\boldsymbol{I(i)-\bar{I}})(\boldsymbol{I(i+\nu)-\bar{I}})}{\boldsymbol{\bar{I}^2}} \qquad [1]$$

where $\tau=\nu*\Delta t_{acq}$, I is the integrated intensity over Δt_{acq} and N is the total number of integrated fluorescence samples. Samples were taken in both real experiments and simulations out to a final time of 30s. The spatial dependence of the emitted fluorescence was described by the following equation;

$$I(x,y,z) = I_o e^{\left(-\frac{2(x^2+y^2)}{r_o^2}\right)} e^{\left(-\frac{2z^2}{z_o^2}\right)} \qquad [2]$$

where I_o was assumed to be equal to 1, $I(x,y,z) > e^{-2}$ was set equal to zero, $r_o=0.6098*\lambda/NA$=0.232μm and $z_o=2*n*\lambda/NA^2$=0.760μm.

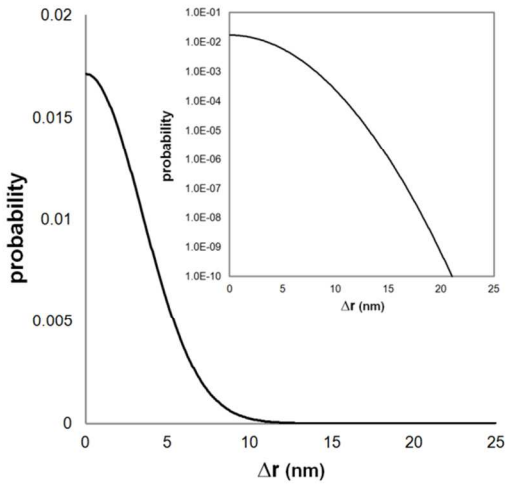

Fig. 2 The probability of a displacement step (Δr) per virtual particle jump time step of Δt for emulating Brownian diffusion. The inset shows the probability axis in *log* scale.

This is the typical expression used when fluctuations in fluorescence quantum yield, the molecular absorption cross-section and detection efficiency are unknown [36]. In the simulation results reported here the single–to–triplet conversion, i.e., fluorescence blinking, was turned off. These features were considered in the simulation described in [36]. Photobleaching was also turned off for the simulations reported here.

A concentration of 101.5 pM (6 virtual particles) was simulated for the case of the 5μm chamber. The virtual particles were distributed randomly within the confines of the chamber for the initial condition at t=0s. A diffusion coefficient of D_o = 371.3 μm^2/s was used to mimic the Brownian motion of the experimentally used AF555 dye. A vector of displacement probabilities $\boldsymbol{P(\Delta r,\Delta t)}$ (equation 3) was used to calculate each particle displacement using a fixed time increment per jump of Δt =15.7ns. Random number sampling, weighted according to this distribution, was used to lookup a unique particle displacement from the vector $\boldsymbol{\Delta r}$ at each time step. The $\boldsymbol{\Delta r}$ vector increment was 0.074nm. Figure 2 shows the resulting digital plot of displacement probabilities. The inset in figure 2 shows the probability axis in *log* form. A random position on the surface of a sphere, with radius Δr, was chosen to completely calculate the 3D position of the diffusing particle.

$$\boldsymbol{P(\Delta r,\Delta t)} = \frac{1}{(4\pi D_o \Delta t)^{3/2}} e^{-\frac{\Delta r^2}{4D_o\Delta t}} \qquad [3]$$

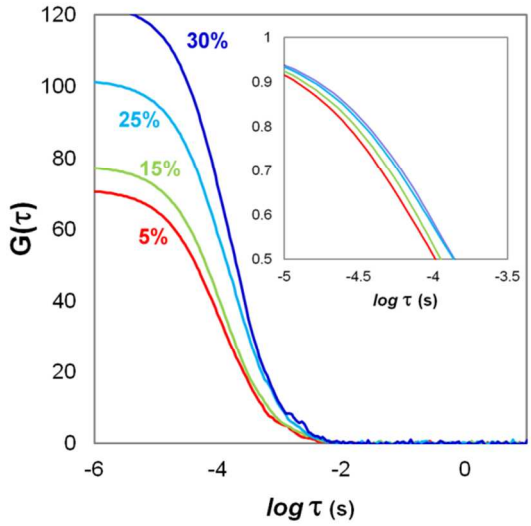

Fig. 3 (a) Fluorescence correlations curves for the cases of 5%, 15%, 25% and 30% volume crowding. These simulations excluded the possibility of particle–wall binding and the beam was centred in the bucket. The inset shows the normalized correlation curves to better emphasize the range of τ_D as a function of crowding percentage.

Particle–wall or particle–lid collisions where considered using the following procedure. After particle displacement, if the particle was within one hydrodynamic radius (R_H =0.74nm) of the wall, or lid, the particle was subsequently placed back into the previous position. The time was advanced Δt with no gross displacement of the particle during that time step. Particle–particle interactions were ignored due to the extremely low concentration of particles in the 5μm bucket ~10^2 pM.

Particle–wall or particle–lid binding events were also included in the simulation by way of a digital switch which could be turned on or off. A binding probability (δ) was considered during each collision. The binding probability was a simulation input variable and ranged from 0–1. A binding event was set to occur according to the following test ($rand < \delta$) when true. Simulations

were executed using δ=0.001. Once bound, during each subsequent random walk time step, the particle was fixed in position and an additional random number based test was used to consider particle–wall or particle–lid desorption. A mean residence time was specified as input (τ_B) and this value was set to 100ms based on experimentally derived desorption times observed for the 5μm diameter bucket case. As a result, the ratio of $\Delta t/\tau$ represents the probability per time step of desorption. The resulting desorption test per walk time step was ($rand < \Delta t/\tau$) with a true result indicating desorption. In our simulation, the assumption was made that bound particles fluoresce with the same probability/efficiency as mobile particles.

Macromolecular crowding was replicated by a simple test ($rand < V_c$), executed per Δt, where V_c is the volume crowding ranging from 0–1. If this condition was true, the particle was held fixed in position in order to emulate a virtual collision with a fictitious crowding obstacle. This simplistic approach was chosen in order to maintain a time tractable simulation – *without* including the crowding effect each simulation required 12–16 hours for completion in order to replicate the experimental intensity acquisition timescale of 30s. Lu et al. have shown the importance of having adequately long FCS acquisition times relative to characteristic decay time of interest [37]. The number of random walk time steps was on the order of ~30s/16ns = $1x10^{10}$ steps. Although a crude emulation of the crowding effect, especially in relation to the method used in [36], the method yielded an FCS curve that was consistent with the FCS curve that was produced when a distribution of static crowding obstacles was placed in the simulation domain. This simplified method used to mimic the nature of a volume crowded solution was deemed a reasonable approach because the characteristic timescale for diffusion, when derived from an FCS experiment, occurs at *~1ms*. This timescale greatly exceeds the timescale (*~10μs*) required for diffusion to become time–independent in a homogeneously crowded solution of Ficoll–70 at 30vol% (S1). Specifically, test simulations revealed that anomalous subdiffusion decays to time–independent, effective diffusion when a particle has diffusively migrated only $(\Delta r^2)^{1/2}$~100nm after *~10μs* (S1). Quantitatively, the random number method used to emulate crowding was found to underestimate the effective diffusion coefficient relative to the more precise simulations which included physical crowding obstacles (S1, *these test simulations implemented the more realistic model for crowding where a random distribution of crowding obstacles is implemented*). Ultimately, it is the relatively large fluorescence excitation beam width used during the FCS experiments that limits the time resolution of diffusion-based information obtainable. For this reason, characteristic diffusion times derived from FCS-based experiments yield the effective diffusion coefficient where increases in crowding closely replicate an increase in the solvent viscosity. In fact, Dauty and Verkman have shown a strong correlation between crowding, macroscopic measurements and diffusion using Ficoll-70 and FCS[30]. However, the interpretation of results, within the simplifying assumptions of the Stokes–Einstein equation $D=k_BT/6\pi R_H\eta$, must be made with care as Dauty and Verkman also point out that results were uncorrelated among diffusion, viscosity and crowding for the case of rhodamine green as a solute where several crowding agents were used including Ficoll 70, albumin and dextran 500kDa[30].

The crowding model including spatially distributed obstacles was executed as follows. . A cubic voxel matrix was overlaid with the cylindrical simulation domain where the voxel spacing was set to equal the hydrodynamic radius of the Ficoll–70 aggregate used to crowd the solution in the complementary real experiments. The binary voxel array was then randomly filled with crowding obstacles according to the desired percent crowded fraction. Each subsequent jump was indexed to this grid and the particle was returned to its initial position if the indexed voxel was occupied, i.e., crowded. Nonetheless, the simulation including the crowding obstacles was error prone considering that (1) a random jump step could be selected, although less probable, that could jump "through" an adjacent crowding obstacle.. As an additional measure of simulation accuracy/relevance, we compared our simulation results, in the form $G(\tau)$ *vs* τ, with those provided in [36] *specifically looking at the increase in* τ_D *as a function of volume crowding.* The characteristic diffusion time τ_D represents the decay in intensity to ½ of the autocorrelation intensity in the anticipated diffusion regime where $\tau_D \sim r_o^2/4D_o$. Figure 3 shows a similar span of τ_D for the simulations reported here and the range shown by [36, figure 8B]. A review of various methods used to emulate the crowding effect on diffusion by simulation can be found in [38].

Results and Discussion

Figure 4 shows a series of panels of normalized FCS measurements taken with AF555 dye in the channel but outside of the femtoliter-volume chambers (panel A), and in chambers decreasing in diameter from 10 μm to 2 μm (panels B-D). In each panel, the effects of increasing amounts of Ficoll-70 crowding agent are shown. Panel E shows the effects of decreasing chamber size at the same crowder concentration. At 50 pM concentration, there are, on average, approximately 10 AF555 molecules in 10 μm chambers (393 fL), 3 molecules in 5 μm chambers (98 fL) and 0.2 molecules in 2 μm chambers (5 fL, most of these chambers will have 0 molecules and a subset will have just one, consistent with a Poisson distribution).[39,40]

Addition of a photobleaching-limiting cocktail to the sample containing glucose oxidase, glucose, catalase and BME, and the ability to close the femtoliter-volume chamber with a well-defined time zero enabled the monitoring of kinetics at early enough times in the compartment for FCS measurements to be carried out (30 seconds). For the smallest chambers (2 μm) the laser intensity had to be reduced by an additional order of magnitude with neutral density filters.

The central result of this paper is the observation of a synergistic, combined effect of increased confinement and crowding on enhanced long lag time correlations, extending past the point where the normalized FCS traces for AF555 molecules outside of the chambers decay to zero (Figure 4, compare panel A with panels B-E). This effect is highlighted in the insets for the panels, each of which includes a rectangular region spanning the range of decorrelation times for AF555 molecules in the bulk solution in panel A, meant to underscore the different behaviour seen in the chambers. While the presence of crowding agent was not needed to observe this effect (i.e., extended lag time correlations were observed in each of the chambers, even at 0%

Ficoll), the addition of crowders amplified it.

X

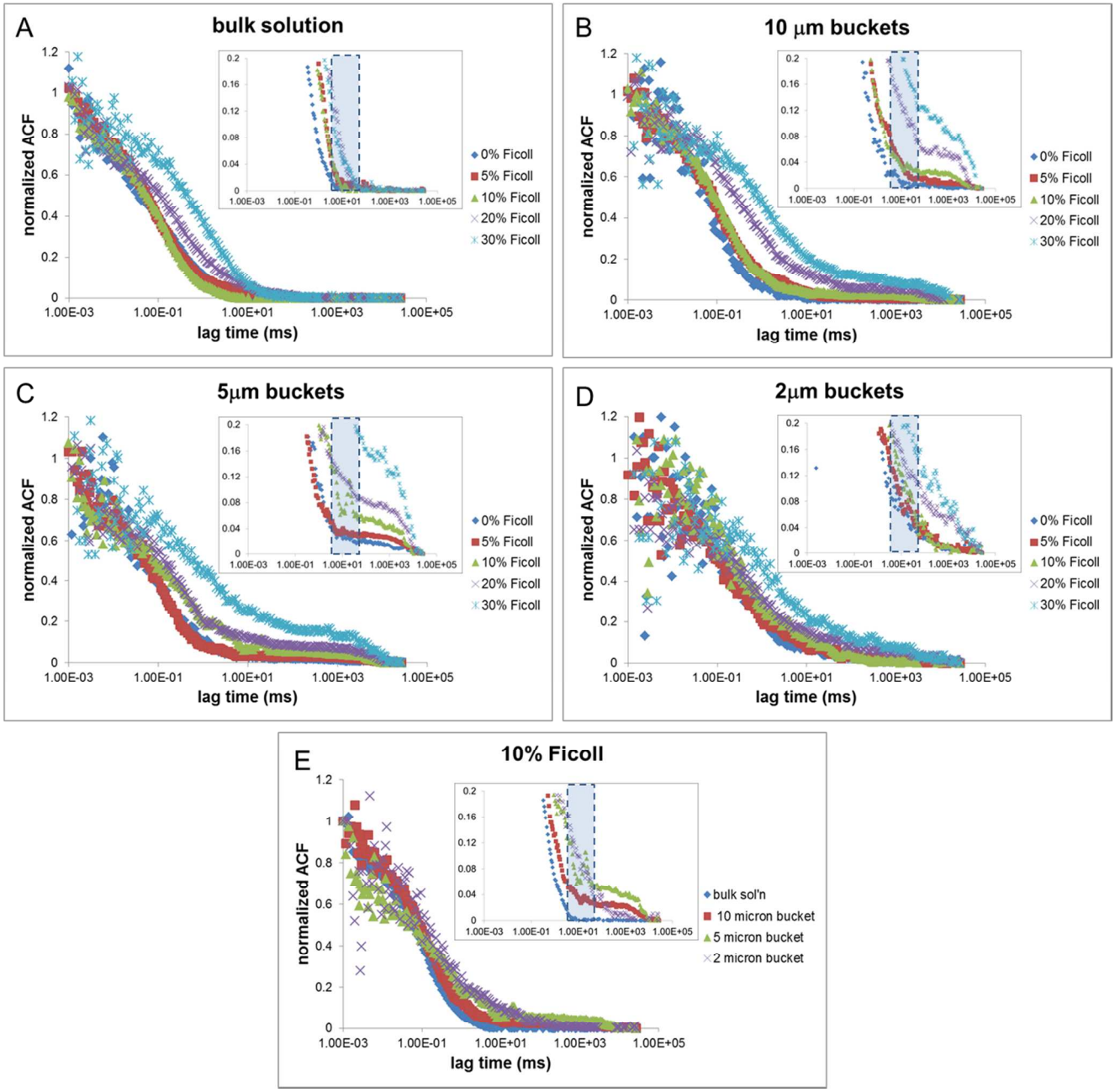

Fig. 4. Series of FCS measurements of AF555 fluorophores in increasingly confined and crowded femtoliter-volume sealed chambers. Insets highlight enhanced long lag time correlations in confined environments (panels B-D,) not observed for fluorophores outside the chambers in bulk solution in the microchannel (panel A). These long lag time correlations were amplified in the presence of crowding molecules like Ficoll-70. Rectangular regions in insets span the range of decorrelation times in bulk solution for increasing Ficoll concentrations, and are meant to underscore the different behaviour in chambers. Panel E shows the effects of decreasing chamber size at the same crowder concentration.

The diffusion times for fluorophores outside the chambers, fit to the standard model for three-dimensional free diffusion, showed a roughly exponential dependence with crowder concentration due to increasing viscosity of the solution, in accord with literature reports.[30]

The Monte Carlo based simulations indicate that observation of this effect is dependent on at least partial intersection of the laser probe volume with a wall. We know from live imaging using the CCD camera during positioning the laser focus in the centre of the chamber that the probe volume did not intersect with the sidewalls. Based on this, our hypothesis is that when the chambers were hydraulically sealed, the lid of a chamber partially deformed and overlapped with the probe volume, which resulted in increased lag time correlations due to emission from fluorophores interacting with the lid.

These effects were amplified as crowding increased, due to local trapping of fluorescent molecules near the lid surface by the crowding fraction. When an adsorbed molecule desorbed from

the lid, there was a higher probability for the molecule to re-adsorb to the surface if it was localized near the lid for long enough times by the crowding molecules.

Particle tracking simulations revealed that fluorescence correlation curves were strongly affected by the position of the laser beam within the confining chamber for the specific case of (1) crowded solutions and (2) surface binding. As one would expect, a surface localized beam is more sensitive to particle–surface interactions although data interpretation must be carefully considered. Significant changes in *G(0)* and the resolution of diffusion/binding correlation times (τ_D , τ_B) were observed if the laser beam was positioned to overlap the lid and interior of the chamber. However, simulations were first explored to determine the effect of increasing the fraction of crowded volume for the beam centred in the chamber.

Fluorescence correlation curves, in terms of τ_D, were found to (1) exhibit an increase in *G(0)* and (2) an increase in the τ_D as the crowding fraction increased. These trends were also consistent with experimental results as well as results reported in the literature.[30] Figure 5a shows the correlation curves for 0% (solid red line) and 23% (solid blue line) crowding, with no binding. The arrow is superimposed to indicate the increase in *G(0)* as crowding increases. An explanation of this trend was found when considering that *G(0)* is inversely proportional to the concentration of fluorescent solute in the chamber. *Evidently, increasing the crowding fraction decreases the range of diffusive exploration for fluorescent molecules – molecules that do not originate within, or in close proximity, to the beam have a reduced probability of exploring this region. An artificially low chamber concentration is suggested by the resulting FCS curve for the 23vol% crowding case.* In the raw intensity versus time data *I(t)* this effect can be seen as a reduced number of intensity spikes (which indicate beam–particle interactions) for the 23% crowded case (S2b), relative to the 0% crowded case (S2a). Further, this explanation suggests that if a molecule were to originate within the confines of the beam at t=0s then the molecule should reside longer in the beam interaction region. This interpretation was confirmed by the observed increase in τ_D with crowding fraction as is routinely observed.[30] This is most easily seen in figure 3 (inset), as the shift to longer lag times of the FCS curve with increasing crowding fraction where the fluorescence correlation curves have been normalized by dividing by *G(0)*. Molecules reside longer in the probe volume in crowded solutions due a lower effective diffusion coefficient ($D < D_o$).

Binding affected the fluorescence correlation negligibly for the centred probe beam scenario (results not shown). Simulations with (1) a crowding range of 0-23% and (2) with particle–lid binding interactions revealed a negligible change in τ_D when compared with complementary simulations with binding off. Apparently, the intense portion of the beam, prone to excite fluorescence at the highest probability, is far enough from the chamber walls nullifying finite boundary effects. *As a result, bound particles are not fluorescently excited and hence do not contribute to acquired correlation curves for a centred laser probe volume.* Only *G(0)* was found to change when including binding; *G(0)* was found to increase for the case of binding. Binding events act to reduce the mobile concentration of particles in the chamber thereby increasing *G(0)*.

On the other hand, fluorescence correlation curves were strongly influenced in response to a displacement of the beam position to the top of the chamber. Simulations were conducted where the beam was centred, in the z–coordinate, at the inner lid surface. The beam was equidistant from the chamber's cylindrical walls. The inset in figure 5 shows schematically this displaced beam configuration (bottom row of inset). Figure 5 shows the FCS results for three identical simulations (red hatched lines) for the 0% volume crowding case with the displaced beam and binding on. These simulation parameters emphasize the effect of confinement (close proximity to chamber surfaces) on both diffusion and binding. It was observed that (1) the apparent concentration of fluorescent particles in the chamber decreased (e.g., the shaded region indicates notable *G(0)* values in figure 5b), (2) a large variation in the shape and form of fluorescence correlation curves was obtained for identical simulation parameters and (3) in some instances the characteristic timescales of diffusion and binding could be separately resolved. A decay at $\tau_B \sim 10^{-1}$s indicated binding (the mean residence time of bound particles was set to 100ms) and the fluorescence decay at $\tau_D \sim 10^{-4}$s was indicative of the diffusion (D_o=371.3 μm^2/s).

The surface localized beam, displaced in position in relation of the centre-of-mass of the fluid in the bucket, made it less probable that molecules would explore the beam, explaining the increase in the mean value of *G(0)* across all hatched red curves shown in figure 5. *I(t)* plots reveal fewer intensity spikes (particle–beam interactions) for the displaced beam (S2c) relative to the centred beam (S2a) at a fixed crowding value of 0.

It may be reasoned that this trend is due to the beam truncation by the lid. Yet, the reflecting boundary condition produces an effective beam size equal to the volume of the centred beam which is confirmed by the nearly constant value of τ_D regardless of whether the beam is positioned at the lid or the centred position. However, the spatial symmetry of the beam–bucket convolution changes in concert with the beam displacement to the lid effectively doubling of the effective bucket volume. This effect is shown schematically in S3. This explains the approximate doubling in *G(0)* in going from the centred (red solid line, figure 5) to the lid displaced beam (figure 5b) at 0% crowding.

The large variation in curve form and shape (*again, with reference to the red hatched curves in figure 5*) is also a result of the stochastic sampling of binding events. Binding events within the beam volume become probable with lid irradiation but were captured with varying degrees of resolution for multiple experiments. For example, the red hatched curve with the lowest value of *G(0)* clearly detected a binding event as evidenced by the clear decay at $\tau_B \sim 10^{-1}$s which strongly effects the curve. In addition, the strong binding sampling increased the apparent concentration in the beam region through lid sticking (red solid line). The remaining two red hatched fluorescence curves sampled fewer particles on average with two binding events evident in the curve labelled (*) and indicated with arrows, while a single binding event was evident for the remaining curve. Thus, the position of the beam within the chamber strongly affects (1) the effective fluorescent particle concentration in the bucket and (2) the ability to resolve diffusion and binding

simultaneously.

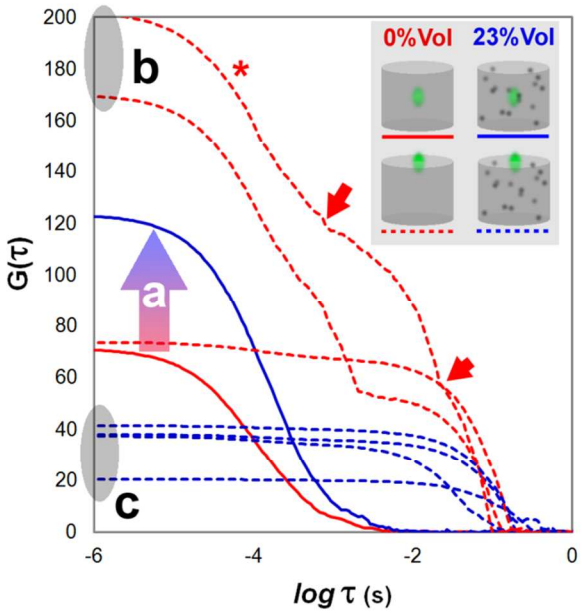

Fig. 5 (a) Fluorescence correlations curves for the cases of 0% (red solid curve) and 23% (blue solid curve) volume crowding. These simulations excluded the possibility of particle–lid binding and the beam was centred in the chamber. (b) Three representative fluorescence curves are shown for the case of 0%volume crowding, a beam position centred on the chamber lid and with binding on (hatched red curves). (c) Four representative fluorescence curves are shown for the case of 23% volume crowding, a beam positioned at the bucket lid and with binding on (hatched blue curves).

Complementary simulations were executed which also included the effect of crowding, using the lid-localized probe volume. *Crowding enhanced the effective binding affinity of the particles to the lids*. For example, the residence time of the particles within the lid-localized, beam probe volume increased as shown by the significantly lower value of *G(0)* for the cluster of simulations at 23% volume crowding (*blue hatched lines, figure 5c*) relative to the 0% crowding case. Considering that the beam–bucket symmetry effect discussed previously (S3) for the displaced beam case alone should *increase,* not decrease, *G(0)* by factor of two. Thus, crowding must be playing a key role in the observed decrease in *G(0)*. *The apparent concentration in the beam region was increased due to crowding but is also convoluted due to the binding of mobile particles at the walls and lids. Specifically, binding in the beam region should decrease G(0) causing an increase in the apparent concentration while binding outside the beam region should increase G(0) causing a real decrease in the mobile, fluorescent concentration.* S2d clearly shows the increased contribution of bound particles to the fluorescence signal as the highlighted yellow regions under the binding signatures in the *I(t)* plot. Additional simulations were also executed which revealed that crowding reduces the number of collisions with wall/lid surfaces (in the absence of binding) yet increases the mean bound fraction (with binding on) through a mechanism of particle-surface interaction which the data shows as coming in bursts of fluorescence intensity (S4). During a burst, once a particle diffuses to a wall/lid, crowding acts to keep the particle close to the wall/lid causing a high density of collisions, or bursts, in time. As a result, large spans of binding activity are observed while particles interact with surfaces. Lastly, regarding binding residence times, a distribution of τ_B decay times about the position $\tau \sim 10^{-1}$s for the multiple simulations conducted, and the case of 23%volume crowding and a displaced beam, reflects the variation of particle desorption in time about the mean, specified value of 100ms.

Conclusions

A microfluidic platform featuring femtoliter-volume, sealable chambers ranging in diameter from 10 to 2 μm that can trap molecules on demand by hydraulically actuating a control valve was developed and tested with FCS. By systematically increasing both the degree of confinement and crowding in the chambers, we observed extended correlation times for fluorescent intensity fluctuations that were greater than varying either confinement or crowding alone. Although partial collapse of the chambers when sealed precluded a systematic study of confinement from the sidewalls as chambers were reduced in diameter, the partial overlap of the lid with the laser probe volume when sealed allowed for the study of the combined effects of crowding and surface binding.

Results from experimental FCS curves consistent with particle tracking simulations lead to the hypothesis that excluded volume effects due to crowding resulted in local trapping of a molecule or molecules at or near the lid compared to dilute solution, and enhanced the effective binding affinity of the particles to the lid. While crowding alone lengthened the free diffusion times of fluorescent molecules, the presence of the confining chamber lid resulted in still longer diffusion times due to coupling to the lid. In addition, the residence time of the particles within the lid-localized beam probe volume increased in the presence of crowders relative to no crowders.

In cells, crowding helps the formation of macromolecular assemblies that rely on weak but specific interactions through excluded volume effects, which provide an entropic driving force for assembly.[32,33] However, detailed quantitative information about the spatial distribution of macromolecules or the state of assembly in the crowded and confined environment of a cell or organelle is still lacking. The FCS data in increasingly confined and crowded chambers described here captures some of the salient features of crowding in cell-like environments, and sets the stage for more sophisticated single-molecule measurements, such as single-pair Fluorescence Resonant Energy Transfer (spFRET), which can be used to directly monitor biopolymer assembly processes in real time.

Acknowledgements

This research was conducted at the Center for Nanophase Materials Sciences, which is sponsored at Oak Ridge National Laboratory by the Scientific User Facilities Division, Office of Basic Energy Sciences, U.S. Department of Energy.

Notes and references

[a] *Center for Nanophase Materials Sciences, Oak Ridge National Laboratory, Oak Ridge Tennessee, 37831, USA. Email: colliercp@ornl.gov*

† Electronic Supplementary Information (ESI) available: information on the time evolution of the diffusion coefficient , fluorescence intensity plots from particle tracking simulations, convolution of the microfabricated chamber and incident focused laser probe in the simulation. See DOI: 10.1039/b000000x/

1 D. Magde, E.L. Elson and W.W. Webb, *Phys. Rev. Lett.* 1972, **29**, 705.
2 E.L. Elson and D. Magde, *Biopolymers* 1974, **13**, 1.
3 S. Aragon and R. Pecora, *J. Chem. Phys.* 1976, **64**, 1791.
4 D. Magde, E.L. Elson and W.W. Webb, *Biopolymers* 1974, **13**, 29.
5 P. Schwille, U. Haupts, S. Maiti and W.W. Webb, *Biophys. J.* 1999, **77**, 2251.
6 K. Bacia and P. Schwille, *Methods* 2003, **29**, 74.
7 T. Wohland, R. Rigler and H. Vogel, *Biophys. J.* 2001, **80**, 2987.
8 C.L. Kuyper, B.S. Fujimoto, Y. Zhao, P.G.Schiro and D.T. Chiu, *J. Phys. Chem. B* 2006, **110**, 24433.
9 T.E. Starr and N.L. Thompson, *Biophys. J.* 2001, **80**, 1575.
10 C.R. Daniels, C. Reznik and C.F. Landes, *Langmuir* 2010, **26**, 4807.
11 O. Krichevsky and G. Bonnet, *Rep. Prog. Phys.* 2002, **65**, 251.
12 R. Rigler and E.S. Elson, *Fluorescence correlation spectroscopy: Genesis, Evolution, Maturation and Prognosis*, 2nd ed.; Springer: Heidelberg, Germany, 2001.
13 A. Gennerich and D. Schild, *Biophys. J.* 2000, **79**, 3294.
14 L. Sanguigno, I. De Santo, F. Causa and P. Netti, *Anal. Chem.* 2010, **82**, 9663.
15 I. von der Hocht and J. Enderlein, *Exp. Mol. Pathol.* 2007, **82**, 142.
16 M. Gösch, H. Blom, J. Holm, T. Heino and R. Rigler, *Anal. Chem.* 2000, **72**, 3260.
17 P.F. Lenne, D. Colombo, H. Giovannini and H. Rigneault, *Single Mol.* 2002, **3**, 194.
18 K.K. Kuricheti, V. Buschmann and K.D. Weston, *Appl. Spectrosc.* 2004, **58**, 1180.
19 P.S. Dittrich and P. Schwille, *Anal. Chem.* 2002, **74**, 4472.
20 S.M. Stavis, J.B. Edel, Y.G. Li, K.T. Samiee, D. Luo and H.G. Craighead, *J. Appl. Phys.* 2005, **98**, 044903.
21 M. Foquet, J. Korlach, W. Zipfel, W.W. Webb and H.G. Craighead, *Anal. Chem.* 2002, **74**, 1415.
22 M. Foquet, J. Korlach, W.R. Zipfel, W.W. Webb and H.G. Craighead, *Anal. Chem.* 2004, **76**, 1618.
23 I. De Santo, F. Causa and P.A. Netti, *Anal. Chem.* 2010 **82**, 997.
24 Z. Petrášek, M. Krishnan, I. Mönch and P. Schwille, *Microsc. Res. Tech.* 2007, **70**, 459.
25 E.B. Gonzales, T. Kawate and E. Gouaux, *Nature* 2009, **460**, 599.
26 L. Wawrezinieck, H. Rigneault, D. Marguet and P.F. Lenne, *Biophys. J.* 2005, **89**, 4029.
27 S.M. Mahurin, S. Dai and M.D. Barnes, *J. Phys. Chem. B* 2003, **107**, 13336.
28 J.C. Gadd, C.L. Kuyper, B.S. Fujimoto, R.W. Allen and D.T. Chiu, *Anal. Chem.* 2008, **80**, 3450.
29 N. Fatin-Rouge, and J. Buffle, *Biophys. J.* 2004, **86**, 2710.
30 E. Dauty and A.S. Verkman, *J. Mol. Recognit.* 2004, **17**, 441.
31 M.A. Unger, H.P. Chou, T. Thorsen, A. Scherer and S.R. Quake, *Science* 2000, **288**, 113.
32 S. Cayley and M.T. Record Jr., *J. Mol. Recognit.* 2004, **17**, 488.
33 S.B. Zimmerman and A.P. Minton, *Annu. Rev. Biomol. Struct.* 1993, **22**, 27.
34 C. Gell, V. Bormuth, G.J. Brouhard, D.N. Cohen, et al., *Method Cell Biol.* 2010, **95**, 221.
35 P.O. Gendron, F. Avaltroni and K.J. Wilkinson, *J. Fluoresc.* 2008, **18**, 1093.
36 J.A. Dix, E.F.Y. Hom and A.S. Verkman *J. Phys. Chem. B* 2006, **110**, 1896.
37 C. –Y. Lu and D. A. Vanden Bout, *J. Chem. Phys.* 2006, **125**, 124701.
38 J.A. Dix and A.S. Verkman *Annu. Rev. Biophys.* 2008, **37**, 247.
39 H.H. Gorris and D.R. Walt, *Angew. Chem. Int. Ed.* 2010, **49**, 3880.
40 S.Y. Jung, Y. Liu and C.P. Collier, *Langmuir* 2008, **24**, 4439.